Analytical pressure-deflection curves for the inflation of pre-stretched circular membranes

Stefano Sirotti[a,b,*], Matteo Pelliciari[a], Angelo Aloisio[c], Angelo Marcello Tarantino[a]

[a] *DIEF, Department of Engineering "Enzo Ferrari", via P. Vivarelli 10, 41125 Modena, Italy*
[b] *College of Civil Engineering, Fuzhou University, No. 2 Xue Yuan Road, 350108 Fuzhou, Fujian Province, PR China*
[c] *Department of Civil, Construction-Architectural and Environmental Engineering, University of l'Aquila, via G. Gronchi 18, 67100 L'Aquila, Italy*

Abstract

The inflation of circular membranes is a benchmark problem in finite elasticity. Due to its mathematical complexity, so far most efforts have been focused on numerical solutions whereas analytical solutions are still lacking. Recently, Pelliciari et al. [1] have proposed an analytical formula for the pressure-deflection relation of circular membranes subjected to inflation. The present work extends that formula to initially stretched membranes. Since the pre-stretch changes qualitatively the pressure-deflection curves, the extension is not trivial and a new analysis is required. The compressible Mooney-Rivlin hyperelastic model is assumed as constitutive law. Following the semi-inverse method, an analytical model assuming spherical deformed configurations is developed and a pressure-deflection relation is derived. Due to the simplifying hypothesis on the kinematics, the analytical expression for the pressure is not always accurate and requires an adjustment. Therefore the pressure-deflection formula is corrected by introducing polynomial functions. The coefficients are calibrated by fitting numerical solutions of the differential equilibrium equations of the exact theory. The calibration is performed over a wide range of material parameters and pre-stretch, covering all the values of practical interest. As a result, an accurate and ready-to-use pressure-deflection relation for practical applications is obtained. The proposed formula is validated by finite element simulations. Differently from other solutions in literature, our formula holds for both compressible and incompressible materials. Experimental bulge tests on pre-stretched rubber membranes are carried out and the proposed formula is used for the calibration of material parameters. A code developed in the software *Mathematica* is made available upon request to directly compute the proposed formula.

Keywords: Pre-stretched membranes; Analytical solutions; Mooney-Rivlin material; Large deformations; Experimental bulge tests.

*Corresponding author. Tel.: +39 3481659986.
Email addresses: stefano.sirotti@unimore.it (Stefano Sirotti), matteo.pelliciari@unimore.it (Matteo Pelliciari),

1. Introduction

Inflation of rubber membranes is employed in many technological applications. This topic assumed great importance in the last few decades and attracted the interest of many researchers from various fields of engineering. Rubber membranes are capable of withstanding very large strains. For this reason, they are used in soft robotics [2–4], dielectric systems [5–7], flexible electronics [8, 9], biomechanics [10–12], and structural and aerospace engineering [13–16].

Both flat, toroidal, spherical and cylindrical membranes have been object of research interest [17–20]. The first theoretical analysis of the inflation of a uniformly thick flat circulare membrane was presented by Adkins and Rivlin [21]. Since then, this problem has received considerable attention. The complexity of this problem in nonlinear elasticity fostered researchers to focus mainly on numerical solutions. Yang & Feng [22] proposed a numerical procedure to solve the boundary-value equilibrium problem of circular inflated membranes characterized by a Mooney-Rivlin material model. DasGupta and Patil [23] extended such numerical solution by introducing a pre-stretch in the initial flat configuration. Later on, Yuan et al. [24] proposed an analytical solution to this problem under strong simplifying assumptions on both the kinematics and the stress state. Recently, Yang et al. [25] proposed a model for pre-stretched flat circular membranes composed of neo-Hookean material, considering in turn simplifying assumptions on the constitutive law.

However, Pelliciari et al. [1] showed that the simplifying hypotheses of such models restrict their validity to limited ranges of material parameters and magnitude of deformation. In particular, in [1], the authors proposed an analytical formula for accurate predictions of the pressure-deflection curve of circular Mooney-Rivlin membranes under uniform lateral pressure. Firstly, a theoretical formula for the pressure-deflection relation was derived under a simplifying hypothesis on the kinematics of deformation. Since this formula was affected by the hypothesis on the kinematics, it was adjusted later by making use of numerical simulations. In particular, the numerical procedure proposed by Yang & Feng [22] was employed to carry out parametric simulations by varying the material parameters. The range of material parameters considered covers the behavior of all rubbers used in technological applications. The final outcome was an adjusted expression of the pressure-deflection relation. Comparisons with finite element (FE) simulations and experiments demonstrated the validity and accuracy of such approach.

The work by Pelliciari et al. [1] was focused on circular flat membranes subjected to inflation. The pre-stretch was not included in the model. However, in engineering applications membranes are in most cases subjected to an in-plane homogeneous pre-stretch before inflation [26]. The presence of a pre-stretch

angelo.aloisio1@univaq.it (Angelo Aloisio), angelomarcello.tarantino@unimore.it (Angelo Marcello Tarantino)

gives an initial out-of-plane stiffness to the membrane and it often improves its performances [27, 28]. The combined effect of inflation and pre-stretch is of much interest in applications such as thermoforming [29] and soft robotics [30]. Considering these practical necessities, accurate analytical solutions of pre-stretched membranes would be of notable importance. Hence, in the present work, we extend the pressure-deflection formula proposed in [1] to the case of pre-stretched membranes. The pre-stretch causes significant qualitative changes in the deformed configurations, in the stretches profiles as well as in the pressure-deflection curves. Therefore, the analytical formula proposed in [1] can not be easily extended, but it is used as a starting point for a new calibration. The proposed formula for pre-stretched membranes is validated by FE simulations. Experimental tests on circular pre-stretched membranes subjected to uniform lateral pressure are presented. It is shown that the formula gives an accurate description of the pressure-deflection response. Moreover, all the other works in the literature consider incompressible materials, an assumption that has not a general validity. Instead, in this work we include compressibility in the material model.

The aim of the present paper is to give an accurate pressure-deflection formula for pre-stretched membranes. The formula is straightforward and can be applied directly without any need of numerical or FE simulations. It will be useful for practical applications and for the estimation of material parameters from experimental biaxial tests. The formulation is implemented in a code in the software Wolfram Mathematica, which can be made available by the authors upon request.

The paper is organized as follows. The theoretical model for circular pre-stretched Mooney-Rivlin membranes under uniform lateral pressure is presented in Section 2. The kinematics of deformation is set a priori and a pressure-deflection relation is derived from the equilibrium. In Section 3 the pressure-deflection formula is adjusted by introducing an additional polynomial function. The coefficients of the polynomial are calibrated by fitting parametric numerical simulations with variations of both material parameters and initial value of pre-stretch. The adjusted formula for the pressure-deflection response is validated with FE simulations, which are described in Section 4. In Section 5 we present experimental bulge tests on pre-stretched circular membranes and we use the proposed model to simulate the pressure-deflection response. Conclusions are drawn in Section 6.

2. Analytical model for pre-stretched circular membranes subjected to inflation

In this section we develop an analytical model for the equilibrium problem of pre-stretched membranes under uniform lateral pressure. The kinematics is described by combining an initial uniform radial stretch and a subsequent inflation, for which it is assumed that the membrane transforms into a spherical cap.

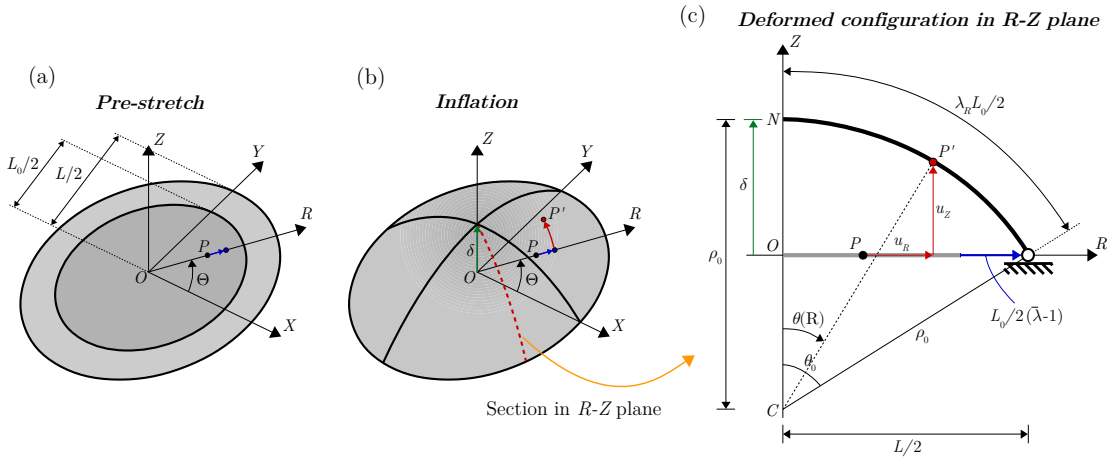

Figure 1: Kinematics of the pre-stretched membrane under uniform lateral pressure p. (a) The membrane is first subjected to a radial pre-stretch $\bar{\lambda} = L/L_0$ and then (b) inflated by a lateral pressure. The cylindrical coordinates (R, Θ, Z) are used as reference system. (c) The deformed membrane maintains rotational symmetry and thus the deformation is described for a generic section in the R-Z plane. After pre-stretch and inflation, a point P moves to P'. The displacement components are u_R and u_Z. The membrane deforms into a spherical cap with radius ρ_0 and central angle θ_0. Parameter θ_0 governs the kinematics. The deflection δ is linked to θ_0 by the relation $\theta_0 = 2\tan^{-1} 2\delta/L$.

The equilibrium is written by adopting a compressible Mooney–Rivlin material model. Finally, a pressure-deflection relation is derived.

We assume that the circular flat membrane has diameter L_0 and thickness H. We define a cylindrical coordinate system (R, Θ, Z) with origin in O. The membrane is first axisymmetrically stretched radially and L indicates the final diameter, as shown in Fig. 1(a). The amount of pre-stretch is given by the ratio $\bar{\lambda} = L/L_0$. In the following, final length L will be held fixed and the pre-stretch will be changed by varying the initial length L_0. The membrane is then inflated under a uniform lateral pressure p (Fig. 1(b)). A generic material point $P \equiv (R, \Theta, 0)$ moves to P', with coordinates (R', Θ, Z'). The deformed configuration is assumed as a spherical cap. The kinematics deriving from this hypothesis is described in Fig. 1(c).

The displacement field $\mathbf{u}(P)$ of point is expressed in cylindrical components as

$$\begin{aligned} u_R(P) &= R' - R = \rho_0 \sin\theta(R) - R, \\ u_\Theta(P) &= 0, \\ u_Z(P) &= Z' = \rho_0 \left[\cos\theta(R) - \cos\theta_0\right], \end{aligned} \tag{1}$$

with $\theta_0 \in (0, \pi)$, $R \in [0, L_0/2]$ and

$$\rho_0 = \frac{L}{2\sin\theta_0}, \qquad \theta(R) = \frac{2\theta_0 R}{L_0}. \tag{2}$$

From now on, the dependence of angle θ on the radial coordinate R is omitted for the sake of simplicity. We

introduce the stretch along the membrane thickness λ_Z. Thereby, thickness H of the undeformed membrane transforms into $H' = \lambda_Z H$ in the deformed configuration. The deformation gradient expressed in cylindrical coordinates is [1]

$$[\mathbf{F}] = \begin{bmatrix} \rho_0 \dfrac{\partial \theta}{\partial R} \cos\theta & 0 & \lambda_Z \sin\theta \\ 0 & \dfrac{\rho_0 \sin\theta}{R} & 0 \\ -\rho_0 \dfrac{\partial \theta}{\partial R} \sin\theta & 0 & \lambda_Z \cos\theta \end{bmatrix}. \tag{3}$$

Reference system (R, Θ, Z) is principal and thus stretches λ_R, λ_Θ and λ_Z are principal. Radial and circumferential stretches are expressed by

$$\lambda_R = \rho_0 \frac{\partial \theta}{\partial R} = \frac{2\theta_0 \rho_0}{L_0}, \qquad \lambda_\Theta = \frac{\rho_0 \sin\theta}{R}. \tag{4}$$

Stretch λ_R is constant because it was assumed that the flat membrane deforms into a spherical cap.

The stored energy function ω of an isotropic material depends only on the principal invariants $\imath_j$ $(j = 1,2,3)$ of the right Cauchy-Green deformation tensor $\mathbf{C} = \mathbf{F}^T\mathbf{F}$ [31], which are defined as:

$$\begin{aligned} \imath_1 &= \lambda_R^2 + \lambda_\Theta^2 + \lambda_Z^2, \\ \imath_2 &= \lambda_R^2\lambda_\Theta^2 + \lambda_R^2\lambda_Z^2 + \lambda_\Theta^2\lambda_Z^2, \\ \imath_3 &= \lambda_R^2\lambda_\Theta^2\lambda_Z^2. \end{aligned} \tag{5}$$

The Biot stress tensor [32] in cylindrical components is

$$[\mathbf{S}] = \begin{bmatrix} S_R & 0 & 0 \\ 0 & S_\Theta & 0 \\ 0 & 0 & S_Z \end{bmatrix}, \tag{6}$$

with

$$S_J = 2\left[\left(\frac{\partial \omega}{\partial \imath_1} + \imath_1 \frac{\partial \omega}{\partial \imath_2}\right)\lambda_J - \frac{\partial \omega}{\partial \imath_2}\lambda_J^3 + \imath_3 \frac{\partial \omega}{\partial \imath_3}\lambda_J^{-1}\right], \quad \text{for } J = R, \Theta, Z. \tag{7}$$

The first Piola-Kirchhoff stress tensor is computed as $\mathbf{T}_R = \mathbf{RS}$, where rotation tensor $\mathbf{R}$ reads

$$[\mathbf{R}] = \begin{bmatrix} \cos\theta & 0 & \sin\theta \\ 0 & 1 & 0 \\ -\sin\theta & 0 & \cos\theta \end{bmatrix}. \tag{8}$$

The Cauchy stress tensor is defined as $\mathbf{T} = (\det\mathbf{F})^{-1}\mathbf{T}_\mathbf{R}\mathbf{F}^T$ [33]. The principal directions (r, θ, z) for the Cauchy stress tensor are obtained through a rotation, given by tensor $\mathbf{R}$, of the material reference system (R, Θ, Z).

The material behavior is defined by the compressible Mooney-Rivlin material model [34, 35]

$$\omega(\imath_1,\imath_2,\imath_3) = a(\imath_1-3)+b(\imath_2-3)+c(\imath_3-1)-(a+2b+c)\ln\imath_3, \tag{9}$$

where parameters a, b and c are positive scalars. Having assumed such stored energy function for the material model, the components of tensor $\mathbf{S}$ are derived by substitution of Eq. (9) into Eq. (7). Consequently, both Piola-Kirchhoff and Cauchy stress measures are computed. The expression of the transversal stretch λ_Z is obtained by imposing the plane stress condition $S_Z = 0$ [1].

The local equilibrium equation for $R \to 0$ gives the following expression for the external pressure

$$p = \frac{2\left(\mathrm{T}_{rr}H'\right)\big|_{R\to 0}}{\rho_0}, \tag{10}$$

with T_{rr} indicating the principal Cauchy stress along direction r and $H' = \lambda_Z H$. Principal stress component T_{rr} for the case of $R \to 0$ reads

$$\mathrm{T}_{rr}\big|_{R\to 0} = \frac{2\sin^2\theta_0\left(\theta_0^2\bar{\lambda}^2\csc^2\theta_0-1\right)\left(a+b\theta_0^2\bar{\lambda}^2\csc^2\theta_0\right)\left[a+2b+\theta_0^2\bar{\lambda}^2\csc^2\theta_0(2b+c)+c\left(1+\theta_0^4\bar{\lambda}^4\csc^4\theta_0\right)\right]}{\theta_0^2\bar{\lambda}^2\sqrt{(a+2b+c)\left(a+2b\theta_0^2\bar{\lambda}^2\csc^2\theta_0+c\theta_0^4\bar{\lambda}^4\csc^4\theta_0\right)}}. \tag{11}$$

Transversal stretch λ_Z assumes the following form with $R \to 0$:

$$\lambda_Z\big|_{R\to 0} = \sqrt{\frac{a+2b+c}{a+2b\theta_0^2\bar{\lambda}^2\csc^2\theta_0+c\theta_0^4\bar{\lambda}^4\csc^4\theta_0}}. \tag{12}$$

We introduce the normalized pressure $\bar{p} = pL/(2aH)$. The expression that links $\bar{p}$ to the kinematic parameter θ_0 is derived by substituting Eqs. (11) and (12) into Eq. (10), obtaining

$$\bar{p} = \frac{4\sin^3\theta_0\left(\theta_0^2\bar{\lambda}^2\csc^2\theta_0-1\right)\left(a+b\theta_0^2\bar{\lambda}^2\csc^2\theta_0\right)\left[a+2b+\theta_0^2\bar{\lambda}^2\csc^2\theta_0(2b+c)+c\left(1+\theta_0^4\bar{\lambda}^4\csc^4\theta_0\right)\right]}{a\,\theta_0^2\bar{\lambda}^2\left(a+2b\theta_0^2\bar{\lambda}^2\csc^2\theta_0+c\theta_0^4\bar{\lambda}^4\csc^4\theta_0\right)}. \tag{13}$$

The kinematics is governed by parameter θ_0 (see Fig. 1(c)), which is related to the displacement δ of the central node of the membrane through the relation $\theta_0 = 2\tan^{-1}\bar{\delta}$, with $\bar{\delta} = 2\delta/L$ indicating the normalized deflection. The expression of pressure $\bar{p}$ given by Eq. (13) can be thus written directly as a function of deflection $\bar{\delta}$. It provides the equilibrium path of the inflated membrane in terms of pressure-deflection curve.

The expression of the pressure for incompressible Mooney-Rivlin materials is derived by computing the limit for $c \to \infty$, which gives

$$\bar{p}\big|_{c\to\infty} = \frac{4\sin^7\theta_0}{\theta_0^6\bar{\lambda}^6}\left(1+\beta\theta_0^2\bar{\lambda}^2\csc^2\theta_0\right)\left(\theta_0^6\bar{\lambda}^6\csc^6\theta_0-1\right) \tag{14}$$

where $\beta = b/a$. In this case β is the only constitutive parameter that affects the response of the membrane

in terms of normalized pressure-deflection curve.

3. Correction of the analytical expression for the pressure-deflection curve

Our proposed model is based on the simplified hypothesis of spherical deformed configurations. The actual deformed configuration depends on the constitutive parameters and on the magnitude of deformation, but generally it is not a spherical cap. As the magnitude of deformation increases, the spherical approximation becomes less accurate leading to significant errors on the pressure-deflection curve. Hence, in the present section we follow the approach proposed by Pelliciari et al. [1] and we correct the analytical expression (14) by introducing an additional polynomial. The polynomial is calibrated on the results obtained from numerical solutions of the exact differential equilibrium equations. This is done for a wide range of values for parameters β and $\bar{\lambda}$, leading to an analytical formula applicable for any circular membrane of practical interest. Firstly we focus our attention on incompressible materials. Later on we generalize the result to the case of compressible materials.

3.1. Numerical solution

The exact differential equations for the equilibrium problem of inflated circular membranes are obtained assuming a general kinematics, namely considering a deformed shape with variable curvature [21–23]. However, a closed-form solution to the governing system of differential equations can not be found and numerical solutions are required. Yang & Feng [22] derived the equilibrium equations for an initially flat and unstretched Mooney-Rivlin membrane, which are expressed by the following system:

$$\begin{aligned}
\lambda_R' &= \frac{\lambda_R\left[3\lambda_\Theta+\lambda_\Theta^3\left(\beta-\lambda_R^4\right)+\lambda_\Theta^4\lambda_R^2 w\left(1-\beta\lambda_R^2\right)+\beta\lambda_\Theta^5\lambda_R^4-w\left(\beta\lambda_R^2+3\right)\right]}{R\lambda_\Theta\left(\beta\lambda_\Theta^2+1\right)\left(\lambda_\Theta^2\lambda_R^4+3\right)},\\
\lambda_\Theta' &= \frac{w-\lambda_\Theta}{R},\\
w' &= \frac{w\lambda_R'}{\lambda_R}-\frac{\psi\lambda_\Theta^3\lambda_R^4\sqrt{\lambda_R^2-w^2}}{2R\left(\beta\lambda_\Theta^2+1\right)\left(\lambda_\Theta^2\lambda_R^4-1\right)}+\frac{\left(\beta\lambda_R^2+1\right)\left(\lambda_\Theta^4\lambda_R^2-1\right)\left(\lambda_R^2-w^2\right)}{R\lambda_\Theta\left(\beta\lambda_\Theta^2+1\right)\left(\lambda_\Theta^2\lambda_R^4-1\right)},
\end{aligned} \tag{15}$$

with $w=\varphi_R'$ and $\psi=pR/aH$. System (15) represents a two-point boundary value problem (TPBVP). In fact λ_Θ is known only at the outer boundary ($\lambda_\Theta(L/2)=1$), whereas at the pole ($R=0$) the principal stretches λ_R and λ_Θ are equal by symmetry. The integration of system (15) is considerably simplified thanks to its invariance property when a scaling factor is multiplied to R. The numerical procedure for the integration of system (15) is described in detail in [1, 22]. After the integration of system (15), the stretches

profiles are obtained for each value of pressure. The deformed coordinates are computed from relations

$$\begin{aligned} \lambda_R &= \sqrt{{\varphi'_R}^2 + {\varphi'_Z}^2}, \\ \lambda_\Theta &= \frac{\varphi_R}{R}, \end{aligned} \tag{16}$$

and the pressure-deflection curve is determined.

The numerical solution outlined by Yang & Feng concerns unstretched membranes, whereas we are dealing with pre-stretched membranes. However, the pre-stretch only affects the boundary condition on λ_Θ, that now reads $\lambda_\Theta(L/2) = \bar{\lambda}$. Therefore, the numerical solution of the equilibrium problem is obtained with the same numerical procedure, but changing the boundary condition.

The constitutive parameters affect the equilibrium equations only through ratio β. For a fixed value of β, variations of parameter a imply only a scaling in the value of pressure. For this reason, it is sufficient to vary β to study the influence of constitutive parameters on the solution. We performed the numerical integration for the same values of β considered in [1], namely for 70 values ranging from 0 to 1. Regarding the pre-stretch $\bar{\lambda}$, we considered 10 values ranging from 1 to 2 with step 0.1. We restricted our interest to these ranges since they are those of practical interest for technological applications [36–39]. For each combination of β and $\bar{\lambda}$, we limited the analysis up to stretches of 6 in any point of the membrane. This choice is consistent with physical evidence, since most rubbers subjected to uniaxial tensile test reach failure for stretches lower than 6 [40]. Besides, in the inflation problem the biaxial strain state arising in each point of the membrane increases the stress demand.

3.2. Fitting to the numerical solution and correction of the pressure-deflection relation

The pressure-deflection relation for unstretched membranes proposed by Pelliciari et al. [1] was

$$\bar{p}_{\text{adj}}\left(\beta,\bar{\delta}\right) = \bar{p}\left(\beta,\bar{\delta}\right) F\left(\beta,\bar{\delta}\right), \tag{17}$$

where $\bar{p}$ is given by Eq. (14) with $\bar{\lambda} = 1$ and $F\left(\beta,\bar{\delta}\right)$ is a polynomial function, expressed by

$$F\left(\beta,\bar{\delta}\right) = \sum_{j=1}^{10} \frac{\bar{\delta}^j}{\bar{\delta}_{max}(\beta)} \sum_{k=0}^{12} d_{jk}\beta^k. \tag{18}$$

Coefficients d_{jk} and function $\bar{\delta}_{max}(\beta)$ can be found in Pelliciari et al. [1]. Eq. (17) was calibrated for $\bar{\lambda} = 1$ and of course is no longer valid if some pre-stretch is considered.

In order to generalize Eq. (17) for pre-stretched membranes, we kept the same form of polynomial $F\left(\beta,\bar{\delta}\right)$, and we assumed that the effect of the pre-stretch can be taken into account by translating the argument in $F\left(\beta,\bar{\delta}\right)$ to $F\left(\beta,\bar{\delta}+\Delta\bar{\delta}\left(\bar{\lambda},\beta\right)\right)$. This approach is based on the qualitative idea that a point

$F\left(\beta,\bar{\delta}+\Delta\bar{\delta}\right)$ on the fitted polynomial corresponds to a more demanding stress state with respect to point $F\left(\beta,\bar{\delta}\right)$. The value of $\Delta\bar{\delta}$ will be such that the increment in the stress state in the interval $F\left(\beta,\bar{\delta}+\Delta\bar{\delta}\right)$ - $F\left(\beta,\bar{\delta}\right)$ corresponds on average to the pre-stress caused by the pre-stretch $\bar{\lambda}$. The increment $\Delta\bar{\delta}$ is not constant but varies for each combination of β and $\bar{\lambda}$. Despite being not rigorous from a mechanical point of view, this approach simplified considerably the fitting procedure preserving a good accuracy.

As further simplification, we assumed that $\Delta\bar{\delta}\left(\bar{\lambda},\beta\right)$ can be expressed as

$$\Delta\bar{\delta}\left(\bar{\lambda},\beta\right)=\psi\left(\bar{\lambda}\right)\phi\left(\beta\right), \tag{19}$$

namely the dependence from $\bar{\lambda}$ and β is contained into two separate functions, $\psi\left(\bar{\lambda}\right)$ and $\phi\left(\beta\right)$ respectively. This assumption corresponds to the intuitive idea that the dependence of the response from β does not change qualitatively for different values of pre-stretch, but only by a scaling factor. This allows to study the dependence from β for a fixed value of pre-stretch, and then to calibrate the function $\psi\left(\bar{\lambda}\right)$. For simplicity we calibrated the function $\phi\left(\beta\right)$ for $\bar{\lambda}=2$, so that $\psi\left(\bar{\lambda}\right)$ is a monotonic function defined in [1,2] with values in [0,1]. For $\bar{\lambda}=2$, $\psi\left(\bar{\lambda}\right)=1$ and $\Delta\bar{\delta}\left(2,\beta\right)=\phi\left(\beta\right)$, while for $\bar{\lambda}=1$, $\psi\left(\bar{\lambda}\right)=0$, $\Delta\bar{\delta}\left(1,\beta\right)=0$ and the expression for unstretched membranes, Eq. (17), is retrieved.

Therefore, we first considered the case of $\bar{\lambda}=2$ and for each value of β_i, $i=1,...,70$, we determined the value ϕ_i such that $\bar{p}_{\text{adj}}\left(\beta_i,\bar{\delta}\right)=\bar{p}\left(\beta_i,\bar{\delta}\right)F\left(\beta_i,\bar{\delta}+\phi_i\right)$ best fitted the numerical solution. We later used the *NonlinearModelFit* function of Wolfram Mathematica to find the best fitting function $\phi\left(\beta\right)$ for the discrete values ϕ_i. Assuming a polynomial expression

$$\phi\left(\beta\right)=\sum_{k=0}^{12}b_k\beta^k, \tag{20}$$

NonlinearModelFit uses a least-square approach to find the set of b_k that best fits the discrete values of ϕ_i. The best fitting coefficients b_k are given in Tab. 1. Finally, we studied the effect of varying the pre-stretch $\bar{\lambda}$. Again, we determined the values ψ_j, $j=1,..,10$, so that

$$\bar{p}_{\text{adj}}\left(\bar{\lambda}_j,\beta,\bar{\delta}\right)=\bar{p}\left(\bar{\lambda}_j,\beta,\bar{\delta}\right)F\left(\beta,\bar{\delta}+\psi_j\,\phi\left(\beta\right)\right) \tag{21}$$

best fitted the numerical solutions for each $\bar{\lambda}_j$ and applied *NonlinearModelFit* to determine the best fitting function of the form

$$\psi\left(\bar{\lambda}\right)=\sum_{k=0}^{3}l_k\bar{\lambda}^k. \tag{22}$$

The estimated coefficients l_k are listed in Tab. 2.

The optimal values ϕ_i and ψ_j and the fitting functions $\phi\left(\beta\right)$ and $\psi\left(\bar{\lambda}\right)$ are shown in Fig 2. Overall, the

Table 1: Coefficients of the polynomial function $\phi(\beta)$ that fit the discrete values ϕ_i.

b_0	b_1	b_2	b_3	b_4	b_5	b_6
b_7	b_8	b_9	b_{10}	b_{11}	b_{12}	
1.07876	40.1897	-620.1	2211.96	16899.7	-199784.4	914510.4
-2.424814×10^6	4.070712×10^6	-4.400039×10^6	2.974882×10^6	-1.146357×10^6	192357.1	

Table 2: Coefficients of the polynomial function $\psi\left(\bar{\lambda}\right)$ that fit the discrete values ψ_j.

l_0	l_1	l_2	l_3
-4.92064	8.34561	-4.15729	0.732323

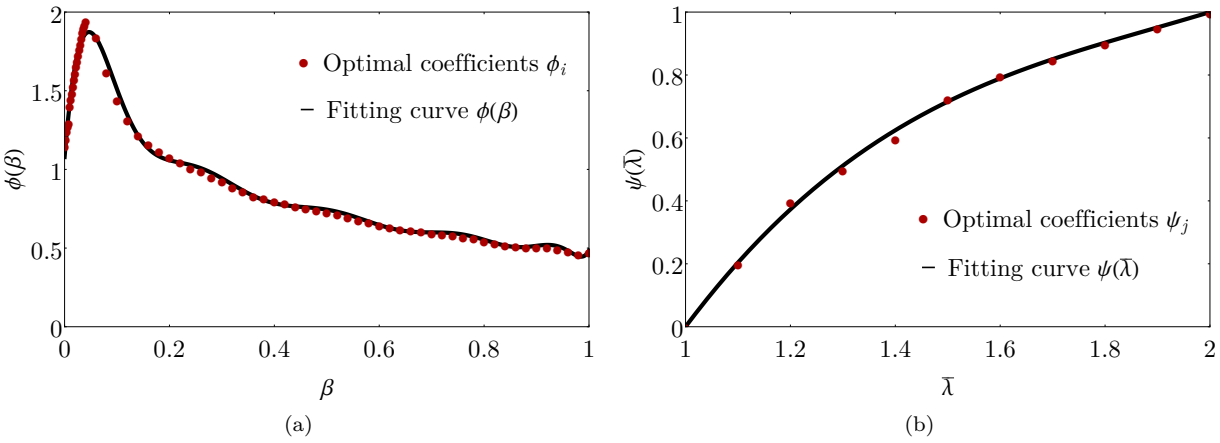

Figure 2: (a) Optimal coefficients ϕ_i for the selected values of β (red dots) and fitting curve $\phi(\beta)$ (continuous line) and (b) optimal coefficients ψ_j for the selected values of $\bar{\lambda}$ (red dots) and fitting curve $\psi(\bar{\lambda})$ (continuous line).

analytical formula for the pressure-deflection relation assumes the following form

$$\bar{p}_{\mathrm{adj}}\left(\bar{\lambda},\beta,\bar{\delta}\right)=\bar{p}\left(\bar{\lambda},\beta,\bar{\delta}\right)\,F\left(\beta,\bar{\delta}+\psi\left(\bar{\lambda}\right)\,\phi\left(\beta\right)\right). \tag{23}$$

Eq. (23) is particularly valuable thanks to its wide range of validity. In fact it gives the normalized pressure and it is indipendent from the constitutive parameter a as well as from the geometrical quantities L and H of the membrane. A variation of these parameters only causes a scaling in the dimensional value of pressure. For this reason, Eq. (23) holds for every circular membrane described by the Mooney-Rivlin constitutive law. Due to the wide ranges considered for β and $\bar{\lambda}$, Eq. (23) covers most cases of practical interest.

Fig. 3 compares the numerical solution and the calibrated analytical formula. The plots are given for $\beta=0.04,0.2,0.5,1$ and for each β the values of pre-stretch $\bar{\lambda}=1,1.2,1.5,2$ are considered. Fig. 4 shows a comparison between the former expression of pressure, Eq. (14), and the adjusted analytical formula, Eq. (23). The plots are given for $\bar{\lambda}=1.5$ and $\bar{\lambda}=2$. For small values of β, the pressure given by the analytical model without any correction results quite accurate even for large deformations. However, for medium and high values of β, as the deformation increases the error committed by Eq. (14) becomes significant and the correction provided by formula (23) is necessary to maintain an accurate prediction of the pressure-deflection response.

4. Validation and discussion

The analytical formula for the pressure-deflection curve calibrated in the previous section is validated by FE simulations. Several values of material parameter β and pre-stretch $\bar{\lambda}$ are considered in order to provide a comprehensive validation. Afterwards, some considerations on neo-Hookean membranes ($\beta=0$) are drawn. Finally, we show that the calibrated formula can be extended to the case of compressible materials in a straightforward manner.

4.1. Finite element simulations

The FE simulations were carried out in COMSOL Multiphysics® version 6.0. The model was built using the 3D membrane interface of the structural mechanics module. The stretched diameter L and thickness H of the membrane were fixed to 100 mm and 1 mm, respectively. The initial diameter L_0 was assigned so that $\frac{L}{L_0}=\bar{\lambda}$. The pre-stretch $\bar{\lambda}$ was enforced by assigning a prescribed displacement to the outer boundary of the membrane. Two values of $\bar{\lambda}$ were considered, $\bar{\lambda}=1.2$ and $\bar{\lambda}=2$. Note that the geometry of the membrane has no influence on the results, since they will be reported in terms of normalized quantities.

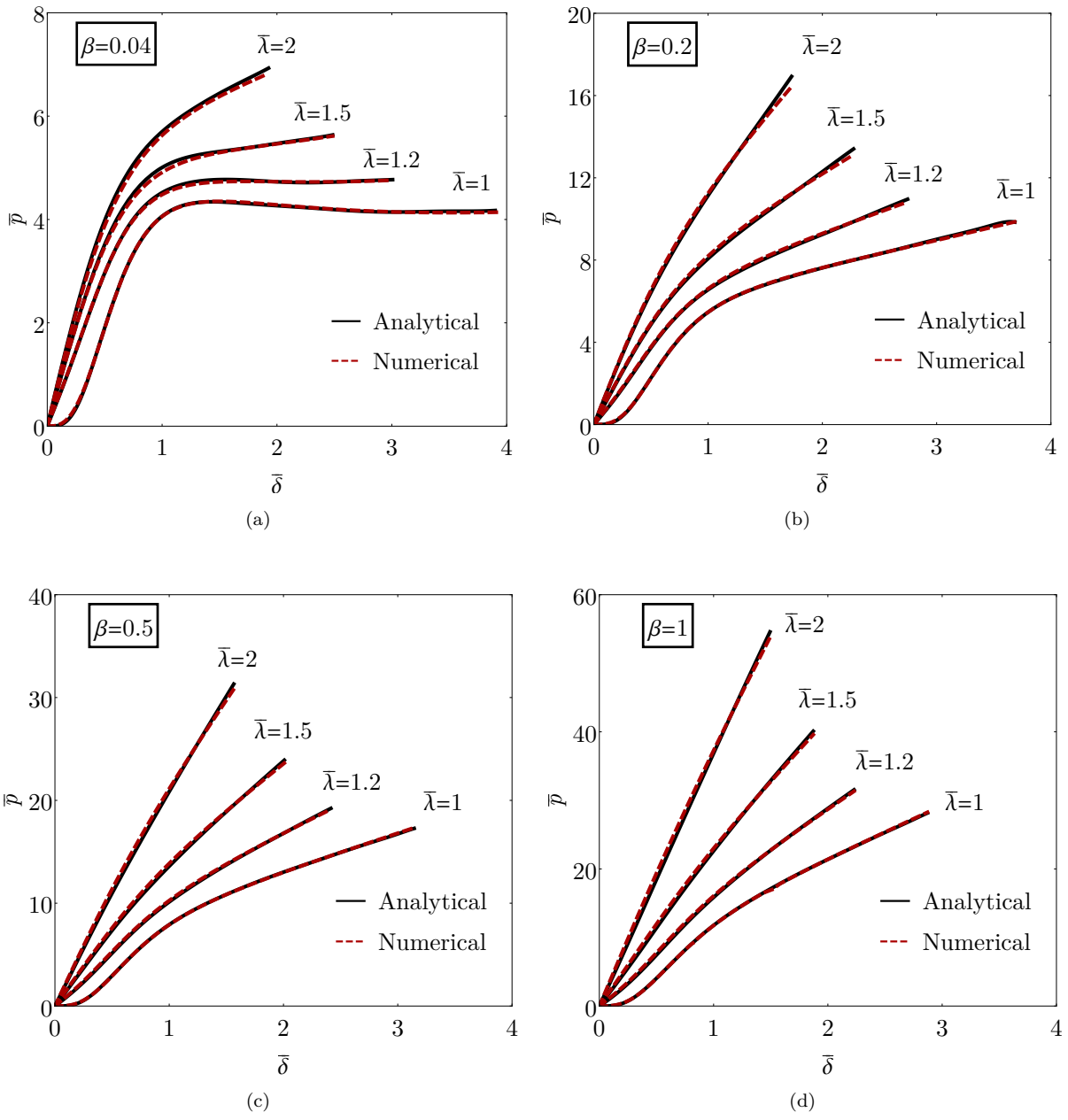

Figure 3: Normalized pressure $\bar{p} = pL/(2aH)$ vs. deflection $\bar{\delta} = 2\delta/L$ curves for different levels of pre-stretch $\bar{\lambda}$: (a) case of $\beta = 0.04$, (b) case of $\beta = 0.2$, (c) case of $\beta = 0.5$ and (d) case of $\beta = 1$. The analytical curves (continuous black lines) are given by Eq. (23).

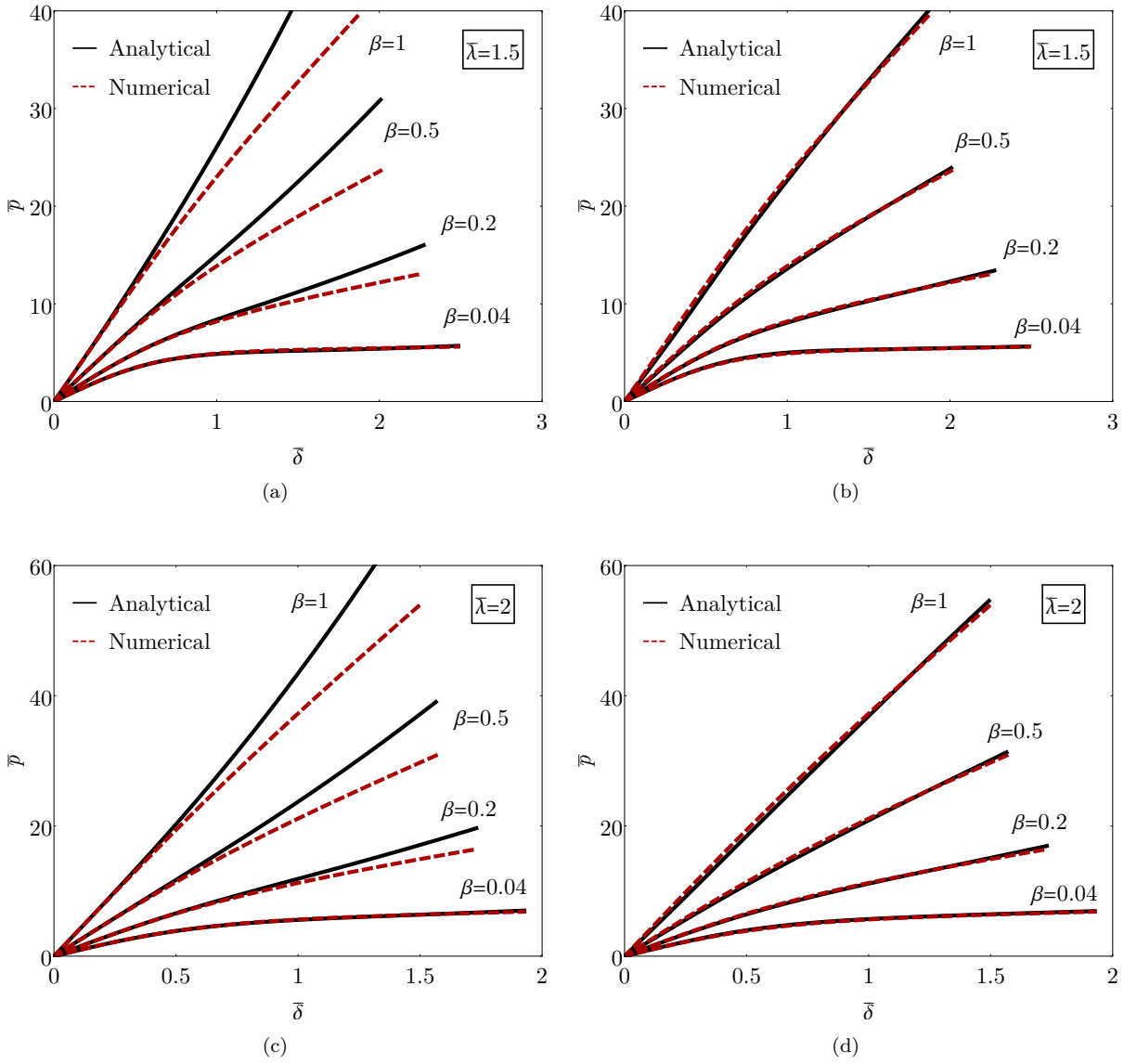

Figure 4: Normalized pressure $\bar{p} = pL/(2aH)$ vs. deflection $\bar{\delta} = 2\delta/L$ curves before and after adjustment: comparison (a) between numerical solution and analytical pressure given by Eq. (14) for $\bar{\lambda} = 1.5$, (b) between numerical solution and analytical pressure given by Eq. (23) for $\bar{\lambda} = 1.5$, (c) between numerical solution and analytical pressure given by Eq. (14) for $\bar{\lambda} = 2$ and (d) between numerical solution and analytical pressure given by Eq. (23) for $\bar{\lambda} = 2$.

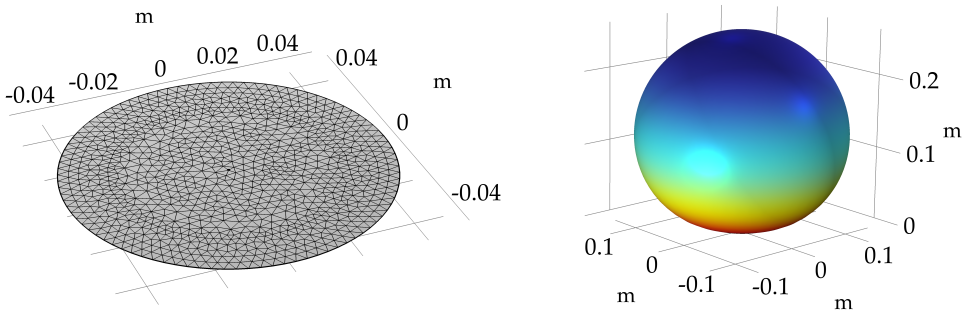

Figure 5: FE model of the inflated membrane: (a) meshed geometry of the membrane and (b) deformed configuration after inflation. The pre-stretch was introduced by applying a prescribed radial displacement to the boundary edge. The built-in two parameter incompressibile Mooney-Rivlin model was chosen as stored energy function. The lateral pressure was increased linearly in a quasi-static manner, considering geometric nonlinearities.

The outer boundary was simply-supported and the two-parameter incompressible Mooney-Rivlin energy function was assigned as constitutive law. Parameter a was set to 1 MPa, while parameter b varies in order to consider different cases of ratio β. In particular, for each value of pre-stretch four cases of β were considered: $\beta = 0.04$ MPa, $\beta = 0.2$ MPa, $\beta = 0.5$ MPa and $\beta = 1$ MPa.

The membrane was discretized in a fine mesh with element size of the order of 0.6 mm (Fig. 5a). The membrane was inflated by a lateral pressure load applied to the free face and increased in a quasi-static manner (Fig. 5b). Geometric nonlinearities must necessarily be considered due to the large deformations involved. The results of the FE simulation are compared with our analytical formula for the pressure-deflection curve in Fig 6. The analytical curves resulted accurate in the entire ranges of deformation and constitutive parameters considered.

4.2. Neo-Hookean material

The case of $\beta = 0$ corresponds to a neo-Hookean material model. In this case, the numerical simulation showed that the deformed configurations tend to spherical caps for increasing values of the pre-stretch $\bar{\lambda}$. For this reason, as $\bar{\lambda}$ increases the simplified model proposed in Section 2 becomes more and more accurate. As a result, Eq. (14) without any correction is sufficient to describe the pressure-deflection relation for neo-Hookean pre-stretched membranes (Fig. 7). This result is consistent with the model proposed by Yang et al. [25], where the authors derived an analytical solution for incompressible neo-Hookean membranes under very large deformations. The following law for the normalized pressure was obtained:

$$\bar{p}_{\text{Yang}} = \frac{8\bar{\delta}}{1+\bar{\delta}^2}. \tag{24}$$

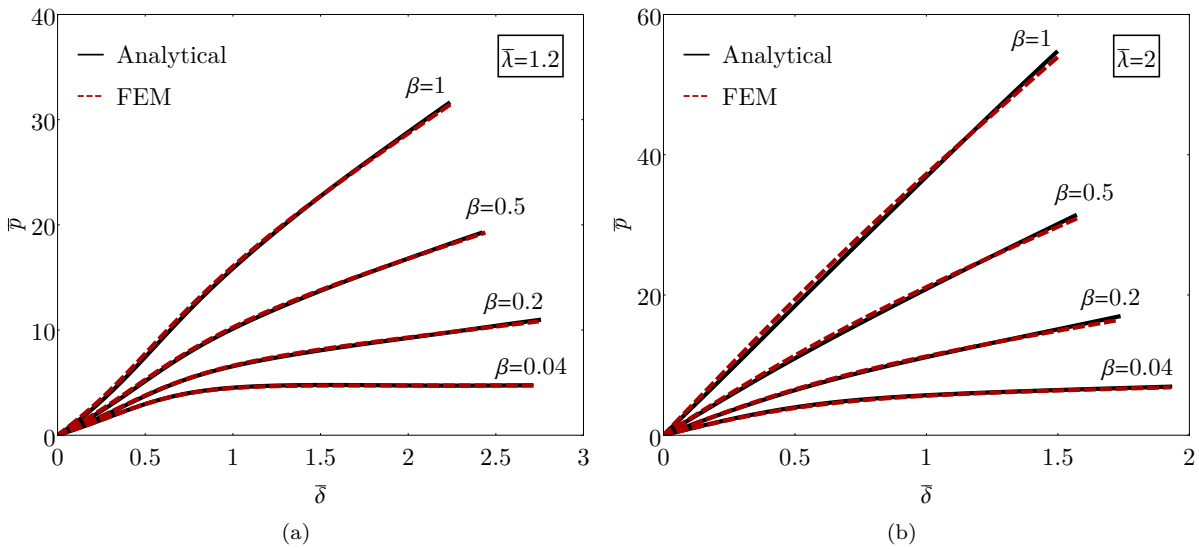

Figure 6: Comparison between normalized pressure $\bar{p} = pL/(2aH)$ vs. deflection $\bar{\delta} = 2\delta/L$ curves given by FE simulations (red dashed lines) and by Eq (23) (continuous black lines) for different values of β: (a) case of $\bar{\lambda} = 1.2$ and (b) case of $\bar{\lambda} = 2$.

Fig. 7 shows that analytical expression (14) matches perfectly the numerical solution even for small values of pre-stretch, while the solution proposed by Yang et al. [25] is accurate only for large values of pre-stretch. This is due to the assumption of very large deformations, which allowed the authors to neglect terms in the equilibrium equations and to derive a closed-form solution. However, for small values of pre-stretch such assumption is not accurate.

In conclusion, we point out that even though Eq. (14) is sufficient for the Neo-Hookean case, the final adjusted expression given by Eq. (23) is accurate as well, as clarified by Fig. 7.

4.3. Compressible materials

In Section 2 we proposed a simplified analytical model for the inflation of membranes under the generic assumption of compressible Mooney-Rivlin material. However, the adjustment of the analytical pressure-deflection relation based on the fitting of numerical solutions was carried out considering incompressible materials. Incompressibility is a well-established assumption for rubbers and rubber-like materials [41, 42]. However, this hypothesis may result inappropriate for some class of materials able to experience large deformations [43–45]. For this reason we now extend our proposed analytical formula to the case of compressible materials.

The extension to compressible materials is immediate provided that Eq. (13) instead of Eq. (14) is used as expression of $\bar{p}$ in Eq. (23). Essentially, the compressibility is already taken into account by the

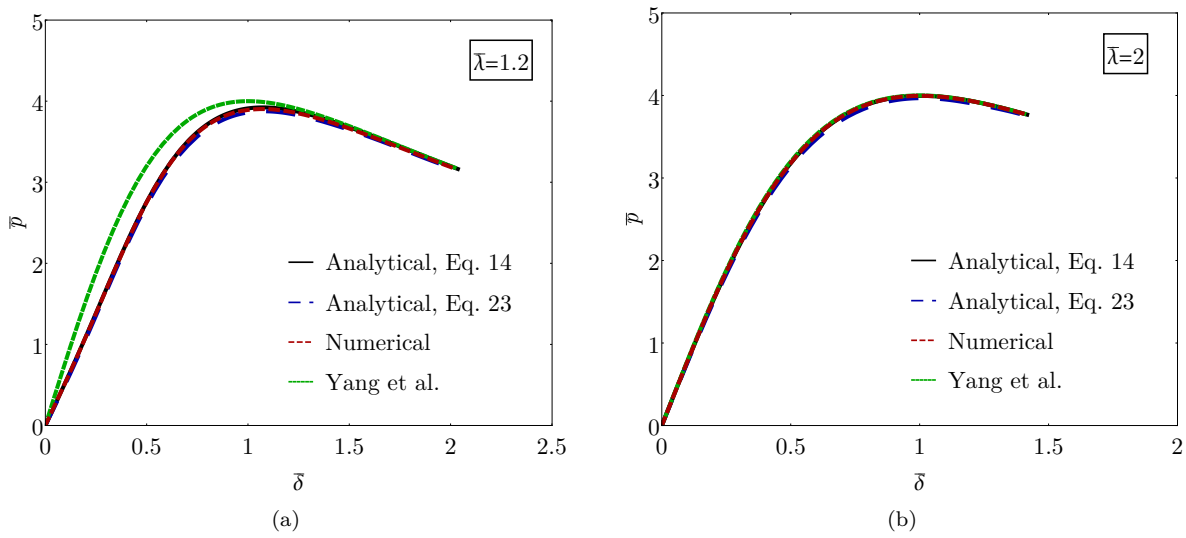

Figure 7: Normalized pressure $\bar{p} = pL/(2aH)$ vs. deflection $\bar{\delta} = 2\delta/L$ curves for Neo-Hookean membranes ($\beta = 0$): (a) case of $\bar{\lambda} = 1.2$ and (b) case of $\bar{\lambda} = 2$. The analytical curves in black continuous lines represent the pressure given by the simplified model described in Section 2 without any correction, the analytical curves in blue dashed lines represent the adjusted pressure after the polynomial correction. For the Neo-Hookean case, both laws are accurate in reproducing the numerical solution. The green dashed lines represent the solution proposed by Yang et al.[25], which is accurate for large values of pre-stretch $\bar{\lambda}$.

analytical model and does not require any special adjusting polynomial. This observation was proved by a comparison with reference numerical solutions. The numerical solutions for compressible materials were obtained following the same procedure described in Pelliciari et al. [1]. Of course, differently from [1] we are now dealing with pre-stretched membranes and the boundary condition becomes $\lambda_\Theta(L/2) = \bar{\lambda}$.

The comparison between analytical and numerical pressure-deflection curves for compressible membranes is shown in Fig. 8. Continuous black lines represent Eq. (23) with $\bar{p}$ given by Eq. (13). Red dashed lines represent the numerical solution for compressible materials and continuous blue lines represent the numerical solution for incompressible materials ($\nu = 0.5$). The curves are given for a pre-stretch $\bar{\lambda} = 1.2$ and two cases of β were considered: $\beta = 0.004$ and $\beta = 0.1$. For each case of β, we selected two values of $\eta = c/a$ such that Poisson's ratio ν equals 0.2 and 0.4. Poisson's ratio is linked to the Mooney-Rivlin constitutive parameters by the following relation [46]

$$\nu = \frac{b+c}{a+3b+2c} = \frac{\beta+\eta}{1+3\beta+2\eta}. \tag{25}$$

It is evident from Fig. 8 that our analytical formula is reliable also for compressible materials. Besides, especially for a moderate magnitude of deformation, there could be some significant difference between the compressible and the incompressible curve. Therefore in some cases the hypothesis of incompressibility should be carefully checked.

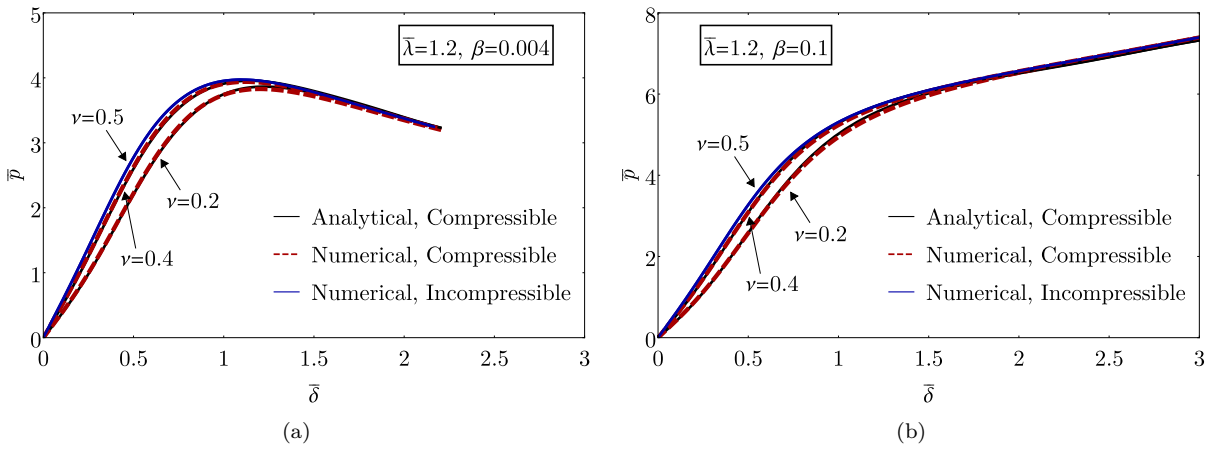

Figure 8: Pressure-deflection curves for compressible membranes with pre-stretch $\bar{\lambda} = 1.2$: (a) $\eta = 0.33$ ($\nu = 0.2$) and $\eta = 2.004$ ($\nu = 0.4$) in the case of $\beta = 0.004$; (b) $\eta = 0.27$ ($\nu = 0.2$) and $\eta = 2.1$ ($\nu = 0.4$) in the case of $\beta = 0.1$. Significant differences between compressible and incompressible materials can be found in the first branch of the curve.

5. Experimental tests

We performed bulge tests on three different rubber sheets considering moderate values of pre-stretch. NBR, silicone and NR were the three rubbers considered. Their thickness was respectively 2, 2 and 1.5 mm. In the following, the setup of the experimental tests is presented and the proposed analytical formula is used for the calibration of the Mooney-Rivlin material parameters for each rubber. Further considerations on the material characterization are discussed by analyzing the uniaxial tensile response of the three rubbers. The experimental data were obtained by carrying out uniaxial tests with the same setup as described in [1].

5.1. Bulge tests

The setup of the tests is shown in Fig. 9. The initially flat circular membrane was inserted into two steel rings that were tightened so that the membrane was fixed. The membrane was placed on a circular steel plate supported by four pillars. The steel plate has a circular hole in the center, with diameter of 15 mm. The rings can slide along four screwed rods and this allowed us to apply a pre-stretching to the membrane. In particular, the value of pre-stretch was set by regulating the position of the rings using 4+4 nuts, placed below and over the rings.

A perforated striking plate was positioned on the membrane. The striking plate was connected to an aluminum tank inside which the external pressure was applied. An hydraulic press was used to push the striking plate against the steel plate and thus avoiding pressure losses. The aluminium tank was pressurized by a low-pressure compressor using an air compression gun equipped with a one-way valve.

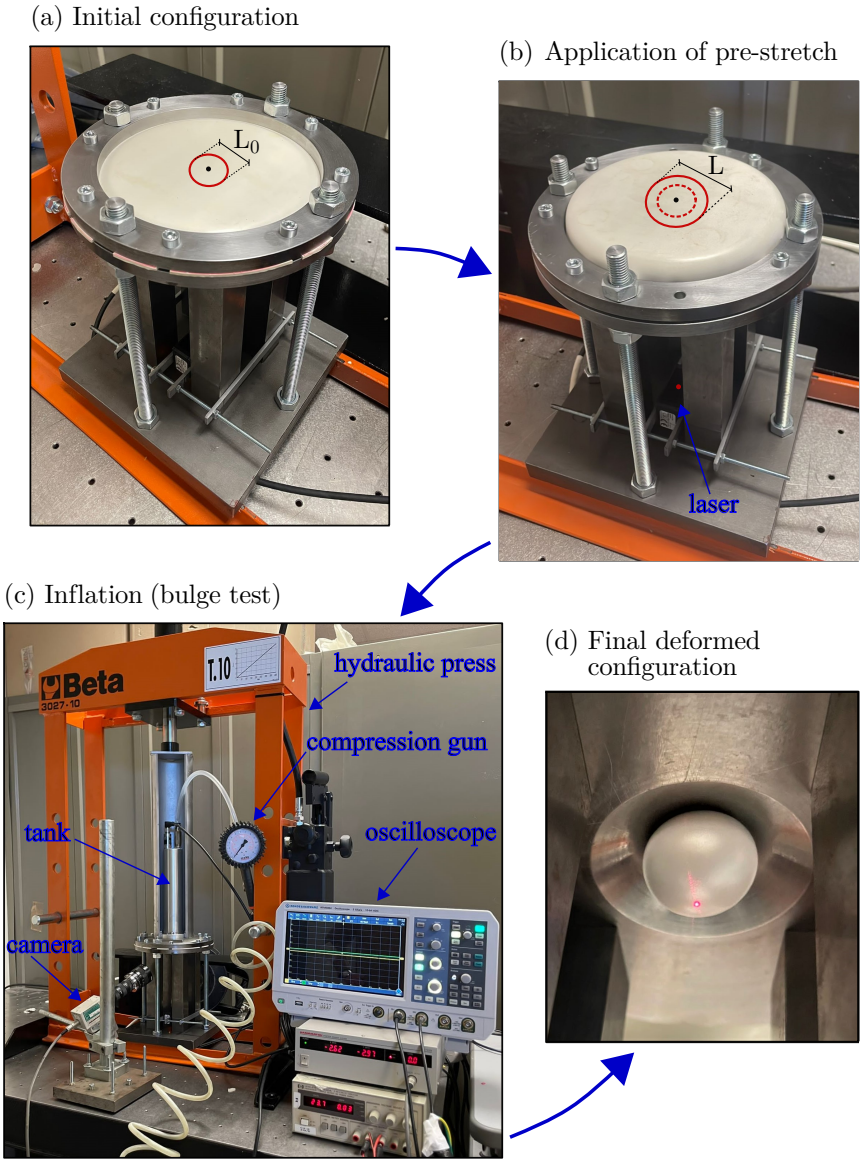

Figure 9: Bulge test. (a) The membrane is placed on a steel plate with a central circular hole. Two steel rings fix the membrane. (b) The rings slide along four screwed rods and stretch the membrane. A laser sensor is placed at the bottom to measure the membrane deflection. (c) A perforated striking plate connected to a tank is positioned on the membrane. A low-pressure compressor injects air into the tank and generates pressure applied on the membrane. (d) Image of the deformed configuration of the circular pre-stretched membrane after inflation.

A pressure reducing valve was used to obtain an applied pressure rate of 0.1 bar/s. The pressure inside the tank was measured using the pressure transmitter TR2101100 produced by Trafag International. The deflection of the central point of the membrane was monitored with the OPTO1420 laser sensor produced by Microepsilon, which was placed at the bottom of the system. The output current signal of both laser sensor and pressure gauge were converted into the corresponding voltage values following a resistive approach. The

Table 3: Values of pre-stretch and Mooney-Rivlin parameters calibrated by fitting experimental data from bulge tests.

	$\bar{\lambda}$	a (MPa)	b (MPa)	β
NBR	1.3	0.5	0.015	0.03
Silicone	1.1	0.55	0.03	0.055
NR	1.2	0.37	0.0296	0.08

Rohde & Schwarz RTM3004 oscilloscope acquired the voltage signals and the data files were then processed using MATLAB, obtaining as outcome the pressure-deflection curve.

For further validation, the membrane deflection was measured by targeting the position of the membrane centre with an optical follower analogue camera (1 Optron 5000 Hz, produced by Hamamatsu). The camera followed the position of the red dot generated by the laser. The output of the camera were two independent signals related to vertical and horizontal components of displacement. This allowed us to cross-check the deflection data from the laser sensor and to make sure that the horizontal component of displacement was negligible.

5.2. Characterization of Mooney-Rivlin constitutive parameters

Quasi-static bulge tests were carried out on NBR, silicone and NR rubber sheets. For each kind of rubber three specimens were tested. Before inflation, the specimens were subjected to a pre-stretch equal to 1.3, 1.1 and 1.2 respectively for NBR, silicone and NR.

After the tests, the experimental curves were fitted to calibrate the material parameters of the Mooney-Rivlin material model. It is well known that, in most cases, the hypothesis of incompressibility is suitable for elastomers. Therefore, in order to simplify the fitting procedure, we adopted such hypothesis. However, our model can be applied to compressible materials and in a general case the accuracy and validity of our hypothesis should be checked. Parameters a and b were calibrated by fitting Eq. (23) to the experimental data from the bulge tests.

The experimental responses and the analytical fitting curves for each rubber are shown in Fig. 10. The calibrated Mooney-Rivlin parameters a and b are reported in Table 3. The analytical formula resulted in excellent agreement with the experimental curves for NBR and silicone. Regarding NR rubber, the analytical curve fits well the experimental response until a stretch approximately equal to 2.5. From that point the experimental response starts to exhibit a hardening trend, typical of some class of polymers for large strains. This behaviour can not be described appropriately by the Mooney-Rivlin model [37], causing a discrepancy between the experimental and analytical curves.

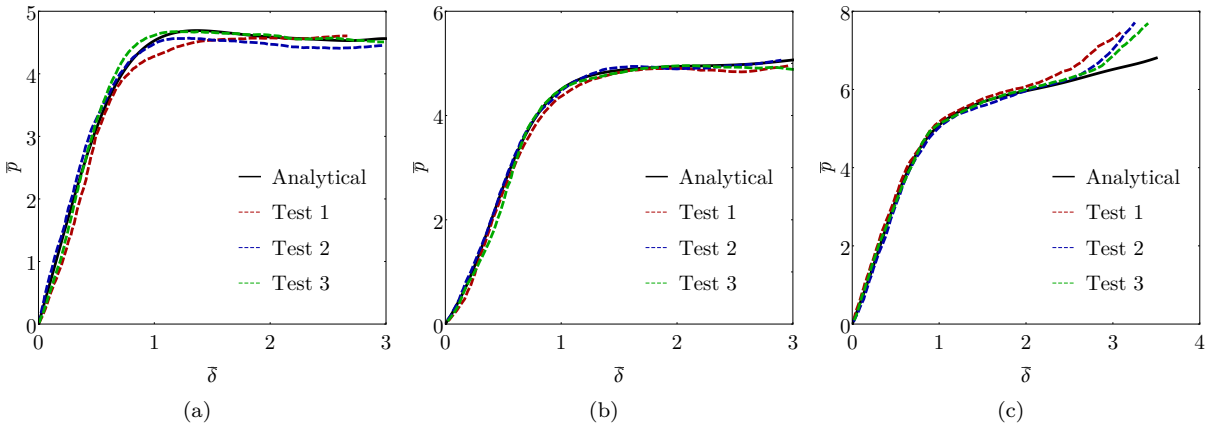

Figure 10: Pressure-deflection curves from bulge tests and comparison with analytical predictions (Eq. (23)) for (a) NBR rubber, (b) silicone rubber and (c) NR rubber. The material parameters used in the analytical formula are listed in Table 3.

Finally, we remark that a set of material parameters calibrated on a determined experimental test cannot be considered representative of the material behaviour in every stress state. On the contrary, its use should be limited to stress states similar to the one of the test used for calibration. In our case the material parameters were determined from bulge tests, so they can give a good representation of the material behaviour under biaxial stress conditions, whereas they are not reliable for other stress states. For instance, we used the parameters calibrated in Table 3 to fit uniaxial tensile tests carried out on the same polymers. The stress-strain relation was obtained from Lanzoni and Tarantino [47], where the authors outlined the analytical model for compressible Mooney-Rivlin solids subjected to uniaxial tractions. Parameter c was set to infinity to consider incompressible material. The results are reported in Fig. 11. It can be observed that the analytical curves with such sets of parameters do not reproduce accurately the experimental uniaxial curves. This shows that material parameters calibrated on biaxial stress states should not be used to predict the response under uniaxial stress states.

6. Conclusions

The aim of this work was to determine an analytical formula for the pressure-deflection curve of inflated pre-stretched membranes in the framework of finite elasticity. Circular flat membranes made of compressible Mooney-Rivlin hyperelastic material were considered. Under the simplifying assumption of spherical deformed configurations, an analytical model for the inflation of membranes was outlined. The equilibrium written at the central point of the membrane allowed us to obtain a pressure-deflection relation.

This expression was affected by the approximation on the kinematics and it was adjusted by a polynomial

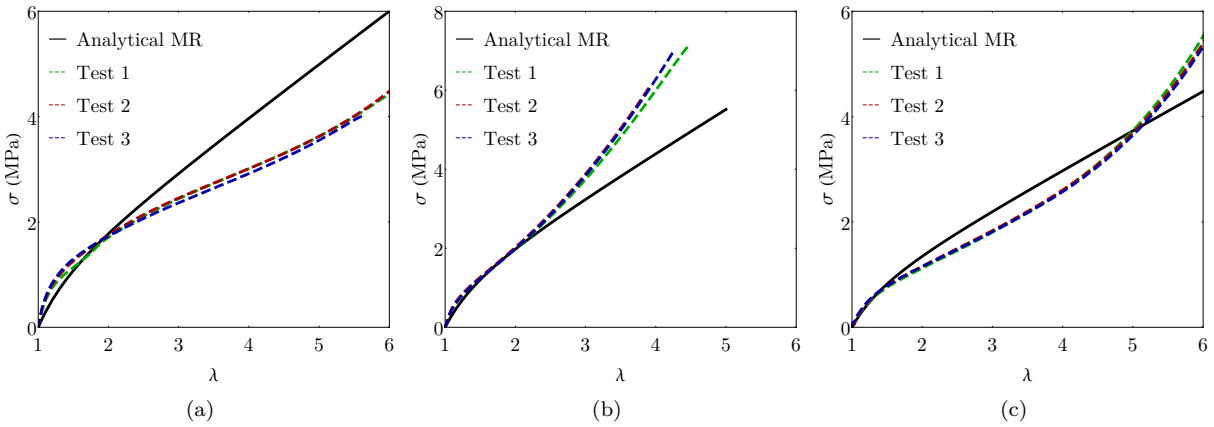

Figure 11: Stress-strain curves from uniaxial tensile tests and comparison with analytical predictions for (a) NBR rubber, (b) silicone rubber and (c) NR rubber. The analytical curves are given by the stress-strain relation for Mooney-Rivlin solids subjected to uniaxial tractions [47]. The parameters used are those calibrated fitting the bulge tests and reported in Table 3, with $c \to \infty$. Being calibrated on different stress conditions, they are not able to give an accurate estimate of the uniaxial response.

fitting of the numerical solution provided by Yang & Feng [22] for incompressible materials. To perform this adjustment, we took advantage of the polynomial function already calibrated in Pelliciari et al. [1] for unstretched membranes. We preserved that polynomial and considered the effect of pre-stretch $\bar{\lambda}$ by introducing two new functions of constitutive parameters β and $\bar{\lambda}$. The coefficients of the corrective functions were determined by fitting the numerical solution for different values of β and $\bar{\lambda}$. As a result, an accurate analytical expression for the pressure-deflection curve of inflated pre-stretched membranes was determined. The proposed formula was validated by FE simulations, obtaining excellent agreement. We then proved our model to be valid also for compressible materials. We showed that variations of parameter c produce significant variations in the pressure-deflection response. Therefore it is important to check the hypothesis of incompressibility commonly adopted for rubber-like materials.

As far as the authors know, few experimental tests on pre-stretched membranes have been carried out, mainly under dynamic electromechanical loading [7, 48]. We filled this void by carrying out bulge tests on three different types of rubbers: NBR, silicone and NR. The proposed analytical formula was used to calibrate the parameters of the incompressible Mooney-Rivlin law on the basis of the experimental data. A good match between experimental and analytical pressure-deflection curves was found for all the materials, except for NR after stretch 2.5. In that case, the experimental curve exhibited a hardening trend which can not be reproduced by the Mooney-Rivlin constitutive law. We showed that the parameters calibrated on bulge tests do not provide accurate results for uniaxial tests, remarking that different stress states require

the calibration of different parameters.

In conclusion, we proposed an analytical formula for the pressure-deflection curve of pre-stretched Mooney-Rivlin membranes that holds for every value of constitutive parameters and pre-stretch of practical interest. Thanks to its simplicity and wide range of validity, the proposed formula is a useful tool for several applications. It may also be used to quickly calibrate the Mooney-Rivlin parameters of rubber-like materials under biaxial stress states.

Future developments on this topic may involve hyperelastic membranes described by more refined constitutive laws. In particular, the attention should be focused on material models able to simulate the hardening that many rubber-like materials exhibit at large deformations.

Acknowledgements

This work was supported by the Italian Ministry of University and Research (MUR) through research grant PRIN 2020 No. 2020EBLPLS on "Opportunities and challenges of nanotechnology in advanced and green construction materials". Support by the National Group of Mathematical Physics (GNFM-INdAM) is also acknowledged.

References

[1] M. Pelliciari, S. Sirotti, A. Aloisio, A. M. Tarantino, Analytical, numerical and experimental study of the finite inflation of circular membranes, International Journal of Mechanical Sciences (2022) 107383.

[2] B. Gorissen, E. Milana, A. Baeyens, E. Broeders, J. Christiaens, K. Collin, D. Reynaerts, M. De Volder, Hardware sequencing of inflatable nonlinear actuators for autonomous soft robots, Advanced Materials 31 (3) (2019) 1804598.

[3] L. Chen, W. Chen, Y. Xue, M. Zhang, X. Chen, X. Cao, Z. Zhang, G. Li, T. Li, Investigation of the state transition and moving boundary in a pneumatic–hydraulic coupled dielectric elastomer actuator, Journal of Applied Mechanics 86 (3) (2019) 031004.

[4] J. Walker, T. Zidek, C. Harbel, S. Yoon, F. S. Strickland, S. Kumar, M. Shin, Soft robotics: a review of recent developments of pneumatic soft actuators, in: Actuators, Vol. 9, Multidisciplinary Digital Publishing Institute, 2020, p. 3.

[5] E. Garnell, C. Rouby, O. Doaré, Dynamics and sound radiation of a dielectric elastomer membrane, Journal of Sound and Vibration 459 (2019) 114836.

[6] N. Goulbourne, E. Mockensturm, M. Frecker, A nonlinear model for dielectric elastomer membranes, Journal of Applied Mechanics 72 (6) (2005) 899–906.

[7] J. W. Fox, N. C. Goulbourne, On the dynamic electromechanical loading of dielectric elastomer membranes, Journal of the Mechanics and Physics of Solids 56 (8) (2008) 2669–2686.

[8] B. G. Stewart, S. K. Sitaraman, Biaxial inflation stretch test for flexible electronics, Advanced Engineering Materials (2021) 2001503.

[9] Z. Liu, A. McBride, B. L. Sharma, P. Steinmann, P. Saxena, Coupled electro-elastic deformation and instabilities of a toroidal membrane, Journal of the Mechanics and Physics of Solids 151 (2021) 104221.

[10] A. Wineman, D. Wilson, J. W. Melvin, Material identification of soft tissue using membrane inflation, Journal of Biomechanics 12 (11) (1979) 841–850.

[11] E. R. Serina, E. Mockensturm, C. D. Mote Jr, D. Rempel, A structural model of the forced compression of the fingertip pulp, Journal of Biomechanics 31 (7) (1998) 639–646.

[12] I. A. Anderson, T. Hale, T. Gisby, T. Inamura, T. McKay, B. O'Brien, S. Walbran, E. P. Calius, A thin membrane artificial muscle rotary motor, Applied Physics A 98 (2010) 75–83.

[13] R. Q. Ma, J. Z. Wei, H. F. Tan, Z. H. Yang, Modal analysis of inflated membrane cone considering pressure follower force effect, Thin-Walled Structures 132 (2018) 596–603.

[14] C. G. Huntington, Tensile fabric structures: design, analysis, and construction, American Society of Civil Engineers, 2013.

[15] C. H. M. Jenkins, Gossamer spacecraft: membrane and inflatable structures technology for space applications, American Institute of Aeronautics and Astronautics, 2001.

[16] W. V. Jones, Evolution of scientific ballooning and its impact on astrophysics research, Advances in Space Research 53 (10) (2014) 1405–1414.
[17] G. Tamadapu, A. DasGupta, Effect of curvature and anisotropy on the finite inflation of a hyperelastic toroidal membrane, European Journal of Mechanics-A/Solids 46 (2014) 106–114.
[18] A. Patil, A. Nordmark, A. Eriksson, Wrinkling of cylindrical membranes with non-uniform thickness, European Journal of Mechanics-A/Solids 54 (2015) 1–10.
[19] A. Needleman, Inflation of spherical rubber balloons, International Journal of Solids and Structures 13 (5) (1977) 409–421.
[20] A. Kydoniefs, A. Spencer, Finite axisymmetric deformations of an initially cylindrical elastic membrane, The Quarterly Journal of Mechanics and Applied Mathematics 22 (1) (1969) 87–95.
[21] J. E. Adkins, R. S. Rivlin, Large elastic deformations of isotropic materials IX. the deformation of thin shells, Philosophical Transactions of the Royal Society of London. Series A, Mathematical and Physical Sciences 244 (1952) 505–531.
[22] W. H. Yang, W. W. Feng, On axisymmetrical deformations of nonlinear membranes, Journal of Applied Mechanics 37 (4) (1970) 1002–1011.
[23] A. Patil, A. DasGupta, Finite inflation of an initially stretched hyperelastic circular membrane, European Journal of Mechanics-A/Solids 41 (2013) 28–36.
[24] J. Yuan, X. Liu, H. Xia, Y. Huang, Analytical solutions for inflation of pre-stretched elastomeric circular membranes under uniform pressure, Theoretical and Applied Mechanics Letters (2021) 100243.
[25] X. Yang, L. Yu, R. Long, Contact mechanics of inflated circular membrane under large deformation: Analytical solutions, International Journal of Solids and Structures 233 (2021) 111222.
[26] H. Vaughan, Pressurising a prestretched membrane to form a paraboloid, International Journal of Engineering Science 18 (1) (1980) 99–107.
[27] S. Akbari, H. R. Shea, An array of 100 μm$\times$ 100 μm dielectric elastomer actuators with 80% strain for tissue engineering applications, Sensors and Actuators A: Physical 186 (2012) 236–241.
[28] A. Saini, D. Ahmad, K. Patra, Electromechanical performance analysis of inflated dielectric elastomer membrane for micro pump applications, in: Electroactive Polymer Actuators and Devices (EAPAD) 2016, Vol. 9798, SPIE, 2016, pp. 180–186.
[29] J. M. Charrier, S. Shrivastava, R. Wu, Free and constrained inflation of elastic membranes in relation to thermoforming–axisymmetric problems, The Journal of Strain Analysis for Engineering Design 22 (2) (1987) 115–125.
[30] Y. Guo, L. Liu, Y. Liu, J. Leng, Review of dielectric elastomer actuators and their applications in soft robots, Advanced Intelligent Systems 3 (10) (2021) 2000282.
[31] R. S. Rivlin, J. L. Ericksen, Stress-deformation relations for isotropic materials, Collected Papers of RS Rivlin (1997) 911–1013.
[32] M. H. Sadd, Continuum Mechanics Modeling of Material Behavior, Academic Press, 2018.
[33] M. Pelliciari, A. M. Tarantino, Equilibrium and stability of anisotropic hyperelastic graphene membranes, Journal of Elasticity 144 (2021) 169–195.
[34] M. Sasso, G. Palmieri, G. Chiappini, D. Amodio, Characterization of hyperelastic rubber-like materials by biaxial and uniaxial stretching tests based on optical methods, Polymer Testing 27 (8) (2008) 995–1004.
[35] N. Kumar, V. V. Rao, Hyperelastic Mooney-Rivlin model: Determination and physical interpretation of material constants, Parameters 2 (10) (2016) 01.
[36] A. P. S. Selvadurai, Deflections of a rubber membrane, Journal of the Mechanics and Physics of Solids 54 (6) (2006) 1093–1119.
[37] G. Marckmann, E. Verron, Comparison of hyperelastic models for rubber-like materials, Rubber chemistry and technology 79 (5) (2006) 835–858.
[38] R. M. Soares, P. B. Gonçalves, Large-amplitude nonlinear vibrations of a Mooney–Rivlin rectangular membrane, Journal of Sound and Vibration 333 (13) (2014) 2920–2935.
[39] T. Gopesh, J. Friend, Facile analytical extraction of the hyperelastic constants for the two-parameter Mooney–Rivlin model from experiments on soft polymers, Soft Robotics 8 (4) (2021) 365–370.
[40] V. P. W. Shim, L. M. Yang, C. T. Lim, P. H. Law, A visco-hyperelastic constitutive model to characterize both tensile and compressive behavior of rubber, Journal of Applied Polymer Science 92 (1) (2004) 523–531.
[41] A. Anssari-Benam, C. O. Horgan, A three-parameter structurally motivated robust constitutive model for isotropic incompressible unfilled and filled rubber-like materials, European Journal of Mechanics-A/Solids 95 (2022) 104605.
[42] H. Khajehsaeid, J. Arghavani, R. Naghdabadi, A hyperelastic constitutive model for rubber-like materials, European Journal of Mechanics-A/Solids 38 (2013) 144–151.
[43] D. Steck, J. Qu, S. B. Kordmahale, D. Tscharnuter, A. Muliana, J. Kameoka, Mechanical responses of ecoflex silicone rubber: Compressible and incompressible behaviors, Journal of Applied Polymer Science 136 (5) (2019) 47025.
[44] Z. Yosibash, I. Manor, I. Gilad, U. Willentz, Experimental evidence of the compressibility of arteries, Journal of the mechanical behavior of biomedical materials 39 (2014) 339–354.
[45] M. Pelliciari, A. M. Tarantino, A nonlinear molecular mechanics model for graphene subjected to large in-plane deformations, International Journal of Engineering Science 167 (2021) 103527.
[46] M. Pelliciari, A. M. Tarantino, Equilibrium paths for von Mises trusses in finite elasticity, Journal of Elasticity 138 (2) (2020) 145–168.
[47] L. Lanzoni, A. M. Tarantino, Equilibrium configurations and stability of a damaged body under uniaxial tractions, Zeitschrift für angewandte Mathematik und Physik 66 (1) (2015) 171–190.
[48] J. Fox, N. Goulbourne, Electric field-induced surface transformations and experimental dynamic characteristics of dielectric elastomer membranes, Journal of the Mechanics and Physics of Solids 57 (8) (2009) 1417–1435.